Geochemistry, Geophysics, Geosystems

RESEARCH ARTICLE
10.1029/2019GC008613

Key Points:
- Authigenic carbonate formation documents episodic methane venting
- Fluid release events respond to uplift and subsidence off Costa Rica
- Diagenetic changes impact sedimentary magnetic signal in non-steady state system

Supporting Information:
- Supporting Information S1

Correspondence to:
N. Riedinger,
natascha.riedinger@okstate.edu

Citation:
Riedinger, N., Torres, M. E., Screaton, E., Solomon, E. A., Kutterolf, S., Schindlbeck-Belo, J., et al (2019). Interplay of Subduction Tectonics, Sedimentation, and Carbon Cycling. *Geochemistry, Geophysics, Geosystems*, *20*. https://doi.org/10.1029/2019GC008613

Received 6 AUG 2019
Accepted 20 SEP 2019

©2019. American Geophysical Union. All Rights Reserved.

Interplay of Subduction Tectonics, Sedimentation, and Carbon Cycling

N. Riedinger[1], M.E. Torres[2], E. Screaton[3], E.A. Solomon[4], S. Kutterolf[5], J. Schindlbeck-Belo[6], M.J. Formolo[7], T.W. Lyons[8], and P. Vannucchi[9,10]

[1]Boone Pickens School of Geology, Oklahoma State University Stillwater, OK, USA, [2]College of Earth, Ocean, and Atmospheric Sciences, Oregon State University, Corvallis, OR, USA, [3]Department of Geological Sciences, University of Florida, Gainesville, FL, USA, [4]School of Oceanography, University of Washington, Seattle, WA, USA, [5]GEOMAR Helmholtz Centre for Ocean Research Kiel, Kiel, Germany, [6]Institute for Geosciences, University of Heidelberg, Heidelberg, Germany, [7]ExxonMobil Upstream Research Company, TX, USA, [8]Department of Earth Sciences, University of California, Riverside, CA, USA, [9]Earth Sciences Department, Royal Holloway, University of London, Egham, UK, [10]Dipartimento di Scienze della Terra, Università degli Studi di Firenze, Firenze, Italy

Abstract Distinct differences were observed in geochemical signatures in sediments from two sites drilled in the upper plate of the Costa Rica margin during Integrated Ocean Drilling Program (IODP) Expedition 334. The upper 80 m at Site U1379, located on the outer shelf, shows pore water non-steady state conditions characteristic of a declining methane flux. These contrast with analyses of the upper sediment layers at the middle slope site (U1378) that reflect steady state conditions. Distinct carbonate-rich horizons up to 11 meters thick were recovered between 63 and 310 meters below seafloor at Site U1379 but were not found at Site U1378. The carbonates and dissolved inorganic carbon from Site U1379 have a depleted carbon stable isotope signal (up to −25‰) that indicates anaerobic methane oxidation. This inference is further supported by distinct δ^{34}S-pyrite and magnetic susceptibility records that reveal fluctuations of the sulfate-methane transition in response to methane flux variations. Tectonic reconstructions of this margin document a marked subsidence event after arrival of the Cocos Ridge, 2.2 ± 0.2 million years ago (Ma), followed by increased sedimentation rates and uplift. As the seafloor at Site U1379 rose from ~2,000 m to the present water depth of ~126 m, the site moved out of the gas hydrate stability zone at ~1.1 Ma, triggering upward methane advection, methane oxidation, and the onset of massive carbonate formation. Younger carbonate occurrences and the non-steady state pore water profiles at Site U1379 reflect continued episodic venting likely modulated by changes in the underlying methane reservoir.

Plain Language Summary Several carbonate-rich layers, up to 11 m in thickness, were recovered in sediments collected at Site U1379 in the outer shelf of the Costa Rica margin, offshore the Osa Peninsula. These layers coincide with minima in the magnetic mineral assemblages. To investigate the processes and mechanisms that led to the formation of these carbonates, we used geochemical and sedimentological analyses of pore water and solid phase samples collected at two sites (U1378 and U1379) during the Integrated Ocean Drilling Program (IODP) Expedition 334. Our results, in the context of available dating and tectonic reconstructions, indicate that the discrete carbonate layers formed near the seafloor driven by anaerobic oxidation of methane, which was released from deeper sediments. The methane discharge events can be related to the subsidence and uplift history of the margin following the subduction of the Cocos Ridge beneath the Caribbean plate. Methane discharge at Site U1379 began ~1.1 Ma, when the ongoing margin uplift brought this site to a depth shallower than that where gas hydrates are stable, breaking a permeability barrier that had kept methane trapped within the sediment. Since then, methane continued to be released in discrete events modulated by characteristics of the gas reservoir.

1. Introduction

Any effort to fully characterize Earth's carbon cycle necessitates a good understanding of the processes that generate and consume methane within the sediment and overlying hydrosphere. Examples in the literature document forcing and consequences of methane advection pulses in sedimentary systems (e.g., Reeburgh, 2007, and references therein). A common approach to unraveling methane dynamics uses the combined

profiles of dissolved sulfate and methane, because the microbially mediated oxidation of methane by sulfate results in characteristic dissolved sulfate profiles that decrease from seawater values to non-detectable sulfate at the sulfate-methane transition (SMT). In the early 1990s, the slope of a linear sulfate profile was shown to be a good indicator of the strength of the methane flow, so that a very shallow SMT would indicate a high methane flux and rapid anaerobic oxidation of methane (AOM; e.g., Niewöhner et al., 1998; Borowski et al., 1999).

We now know that not all pore water sulfate gradients are linear and that deviations from this steady state condition most often reflect recent changes in methane flux, which have been attributed to a gamut of processes including pulses in organic carbon accumulation, mass transport deposition, earthquake activity, and dynamics of deeper methane reservoirs (e.g., Egger et al., 2018; Hensen et al., 2003; Riedinger et al., 2005). We also know that AOM is accompanied by: (1) an increase in alkalinity that promotes precipitation of methane-derived authigenic carbonate (MDAC) and (2) production of H_2S and associated sulfide mineral diagenesis that overprints the magnetic susceptibility of the sediment (e.g., Karlin & Levi, 1983; Tarduno, 1994; Roberts et al., 1999; Neretin et al., 2004; Riedinger et al., 2005, 2017; März et al., 2008; Rowan et al., 2009). These minerals remain in the sediment record and offer an excellent opportunity to reconstruct the history and nature of fluid flow. Examples include studies of modern and paleo-seep carbonate (e.g., Han et al., 2014; Joseph et al., 2013; Pierre et al., 2012) and iron minerals (e.g., Dewangan et al., 2013; Zhang et al., 2014) worldwide.

One of the goals of the Integrated Ocean Drilling Program (IODP) Costa Rica Seismogenesis Project (CRISP) was to investigate fluid flow and related diagenetic reactions on an active margin characterized by erosive subduction processes. Here we report on pore fluids, solid-phase iron, and carbonate phases from IODP Expedition 334. We use our data to relate carbon cycling to the tectonic history of the erosional convergent margin of Costa Rica. We review and update our understanding of the tectonic evolution of the margin using pore water, solid phase, and mineral (carbonate and sulfide) geochemical data complemented with available magnetic susceptibility records. We integrate these results with a modeled gas hydrate stability response to the uplift/subsidence of the forearc basin at, and following, the arrival of the Cocos Ridge, to generate an integrated view of the volatile recycling history of the margin over the past approximately 2 million years. Collectively our results document the timing and effect of fluid release events in response to uplift and subsidence of the margin as the Cocos Ridge subducts offshore the Osa Peninsula.

1.1. Study Area

The CRISP study area (Figure 1a) is located offshore the Osa Peninsula within an area of active and long-lived subduction erosion—that is the removal of crust from the overriding tectonic plate due to subduction of oceanic crust—that extends from Guatemala to Costa Rica (e.g., LaFemina et al., 2009; Ranero et al., 2008; Ranero & von Huene, 2000; Vannucchi et al., 2004, 2013). A well-characterized suture in the incoming plate offshore the Nicoya Peninsula separates the ~24 Ma crust originating at Cocos-Nazca spreading center to the southeast from the similarly aged East Pacific Rise crust that subducts to the northwest of the suture. Seepage in the northwestern region of the forearc is typically focused on cone-shaped mounds with a few localized sites associated with normal faulting (Sahling et al., 2008). In contrast, the forearc segment to the southeast of the plate suture exhibits diverse seep structures that reflect the irregular morphology of the forearc caused by the subduction of ridges and seamounts. Seepage here has been associated with fractures directly related to seamount subduction, mounds, and landslide scars forming preferential fluid migration pathways that commonly control the seepage site (e.g., Kutterolf et al., 2008; Moerz et al., 2005). A more thorough picture of the seep distribution has been developed with the onset of coupled seismic reflection and multibeam surveys that can image gas plumes in the water column (Figure 1c).

Using hull-mounted multibeam and towed side-scan surveys, Sahling et al. (2008) suggested that the location of seepage in this region is centered 28 ± 7 km landward of the trench. In a coupled high-resolution seismic reflection and multibeam survey focused in the region offshore Osa Peninsula, Kluesner et al. (2013) documented a substantially greater seep density over a broader depth range than previously reported, with 161 sites of potential fluid seepage on the shelf and slope regions that had not been detected before (Figure 1a). In this latter study, the authors clearly showed how the seep distribution is controlled by faulting. Fluid seepage indicators include pockmarks, mounds, and ridges ranging from a few meters to hundreds of meters across (Kluesner et al., 2013). Similar to the observations of Sahling et al. (2008), Kluesner et al.

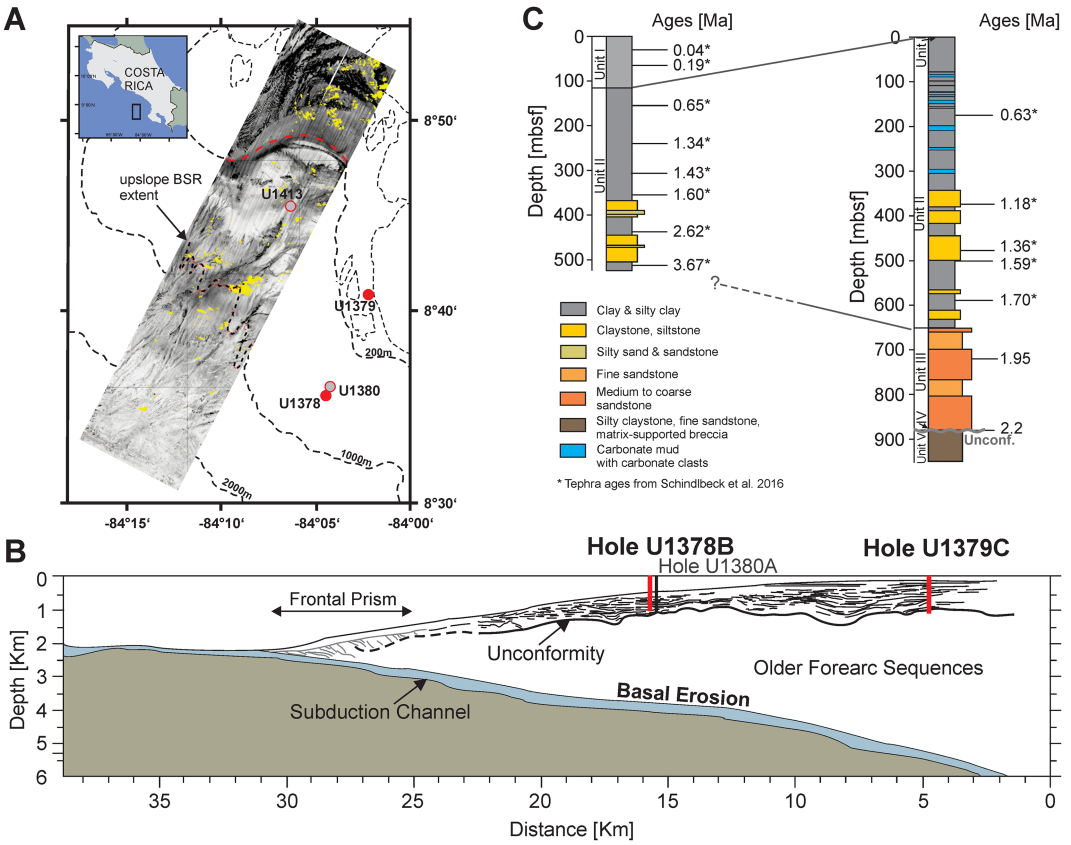

Figure 1. Overview of the study area and drilled sites. (a) Location of study Sites U1378 (127 meters below sea level (m bsl)) and U1379 (522 m bsl) as well as Sites U1380 (504 m bsl) and U1413 (540 m bsl), in the context of a backscatter mosaic of the wide CRISP survey area; the yellow patches on the backscatter patch present potential locations of pockmarks (modified after Kluesner et al., 2013). Simplified seismic cross section along the margin off Costa Rica including the location of the drilled sites (modified after Vannucchi et al., 2012,). (c) Lithology and ages for Sites U1378 and U1379 (modified after Vannucchi et al., 2012 and tephra ages (*) from Schindlbeck et al., 2016a).

(2013) reported seepage across the mid-slope region, coincident with the upper edge of gas hydrate stability, with almost no seep evidence in the lower slope region. These authors also note that the majority of pockmarks observed in the upper and lower slope are associated with BSR weakening and terminations. These observations, tied to a significant decrease in seep density in sediments that lie within the gas hydrate stability zone (Kluesner et al., 2013), are consistent with gas accumulations beneath a zone where interconnected networks of gas hydrate cut off pore space connectivity limiting upward methane advection (e.g., Evrenos et al., 1971; Riedel et al., 2006; Sahoo et al., 2018).

Drilling offshore the Osa Peninsula during IODP CRISP Expeditions 334 and 344 (Figure 1b) probed the nature of the modern forearc sediment apron and the sediment sequence beneath a prominent reflector in the 3-D seismic volume. This reflector extends from the middle slope to the shelf and has been interpreted as a regional angular unconformity (Harris et al., 2013; Vannucchi et al., 2012). The shallowest site along the CRISP transect, Site U1379, was drilled into the outer shelf of the Costa Rica margin with a present seafloor depth of 127 meters below sea level (m bsl). Coring recovered ~1 meter of medium- to coarse-grained beach sand with disarticulated shell fragments (Lithologic Unit I) above the sediments of Lithologic Unit II (0.93–651 m below sea floor, m bsf). These are predominantly monotonous sequences of silty clay to clay that alternates with widely interspersed decimeter-scale sandy layers and abundant tephra layers that remain unlithified to 650 m bsf and are excellent markers for time constraints (Schindlbeck et al., 2016a; Figure 2c). Carbonates occur as discrete concretions and or carbonate mud sediment between 63–305 m bsf (Figure 1c). The carbonate-rich intervals are separated by monotonous silty clay (stone)–clay (stone) and clayey silt (stone)–sand (stone).

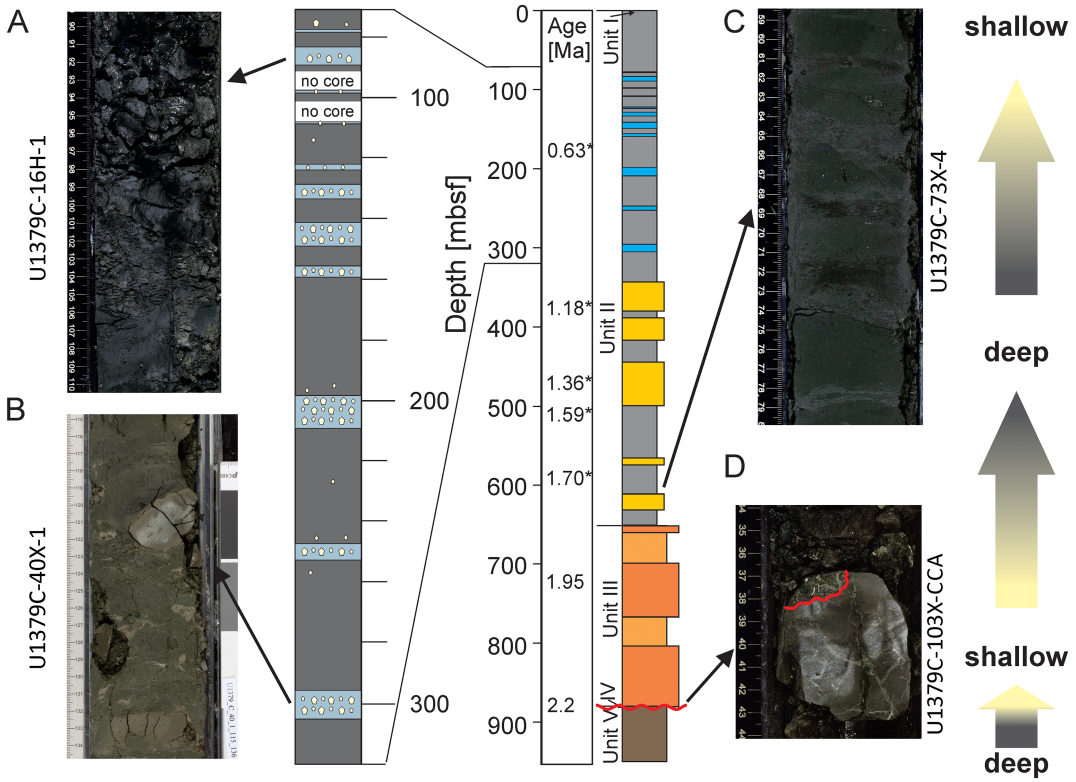

Figure 2. (a and b) Selected core images of carbonate layers from the upper 320 m bsf (for lithology legend see Figure 1). (c and d) Changes from deep marine to shallow marine to deep marine and shallow marine environment is recorded in the cored sediments. The contact between deep marine (Unit V; brecciated mudstone) and shallow marine deposits (Unit IV; bioturbated sands with shell fragments) is indicated by the red line marking the unconformity (modified after Vannucchi et al., 2013).

Olive-green silty sands and sandstone deposits constitute ~64% of the thickness of Lithologic Unit III (651–880 m bsf) and alternate with finer hemipelagic sediments. Small, disseminated wood and plant debris are recognized throughout coarser horizons. Tephra layers are less common than in overlying units. Unit IV (870–882 m bsf) consists of carbonate-cemented medium- to coarse-grained sand containing abundant disseminated shell debris. The basal meter of the unit revealed distinct centimeter-thick shell layers and localized well-rounded pebble conglomerates. The mudstone of Unit V (882–947 m bsf) is brecciated and intercalated with basalt clasts in the upper part, with a sequence of variably sandy and clayey silt matrix in the lower portion (Vannucchi et al., 2012; Figure 1c).

The upper slope was sampled by drilling Site U1378 in 522 m of water, 41 km offshore the Osa Peninsula (Figure 1b). The sediments recovered at this location—a monotonous sequence of silty clay to clay that alternates with widely interspersed centimeter-scale sandy layers—are divided into two main lithostratigraphic units (Figure 1c). Unit I (0–128 m bsf) consists mainly of dark greenish gray, soft, silty clay sediments with 21 tephra layers and is punctuated by thick sequences of lithic sands. Unit II (128–513 m bsf) is a monotonous massive sequence of olive green clay and silt with minor sandy intervals that become thicker and more common with greater depth. The sediment is generally well-consolidated but contains tephra layers that remain unlithified to 506 m bsf (Figure 1c). Drilling at Site U1378 was terminated before reaching the depth of the unconformity, and an additional site, U1380, was drilled to investigate the deeper portions of the upper slope sequence and underlying wedge sediments. The sedimentary succession recovered from the framework wedge at Site U1380 revealed an alternating terrestrially sourced, turbiditic upper slope (Units I, 438 to 553 m bsf, and Unit III, 7,812 to 800 m bsf) to shelf (Unit II, 553 to 772 m bsf) sequence thought to reflect the influence of deltaic-derived sediments (Harris et al., 2013).

The unconformity imaged in the seismic data was sampled at Sites U1379 and U1380 and was found to correspond with a sharp depositional and lithological change dated at 2.2 ± 0.2 Ma. Shell-rich material was

recovered at the unconformity and separates the shallow water base of the modern slope sediment drape from underlying poorly deformed fine- to coarse-grained volcanoclastic turbidites and hemipelagites typical of a deep-water environment (Vannucchi et al.,). The sediments below the unconformity are interpreted as the topmost portion of the wedge imaged in seismic profiles and characterized by a progressive increase in deformation at depth within the wedge itself. Prior to drilling, the material beneath the unconformity was postulated to be crystalline basement, and it was unclear how the fluids from the underthrusting material could provide enough water, and more problematically enough carbon, to support the widespread fluid and methane seepage along this margin (e.g., Bohrmann et al., 2002; Mau et al., 2006; Mau et al., 2007). We now know that the wedge itself generates additional fluids and volatiles (such as methane). Two distinct fluid migration paths were identified from the CRISP pore water data set: (1) lateral advection along the unconformity of deep-sourced fluids consisting of thermogenic hydrocarbons with a fluid composition that indicates source temperatures of at least 90oC (Vannucchi et al., 2012) and (2) a more pervasive migration of dehydration-derived fluids with a distinctly different fluid composition that likely originates from a more local, lower temperature source in the wedge (Harris et al., 2013; Vannucchi et al., 2012).

2. Materials and Methods

2.1. Sampling and Shipboard Analyses

Immediately after core retrieval, a 3-cm^3 bulk sediment sample was collected for headspace analyses from the freshly exposed end of top core sections adjacent to the interstitial water sample. Hydrocarbon composition was measured at sea using an Agilent/HP 6890 Series II gas chromatograph (GC3). The concentrations were subsequently corrected for sediment porosity (Expedition 334 Scientists, 2012). Solid phase and pore water samples were taken from whole-round cores cut and processed immediately after retrieval. Samples were squeezed for pore water, and the extracted pore fluids were treated and stored cool (+4°C). The remaining solid phase (squeeze cake) was stored frozen (−20°C) for further analyses. For detailed description of sampling, sample processing, and analyzes on board the D/V Joides Resolution see the "Methods" chapter (Expedition 334 Scientists, 2012).

2.2. Pore Water and Gas Analyses

Pore water sulfate (SO_4), alkalinity, dissolved calcium (Ca), and methane (CH_4) were measured onboard the DV JOIDES Resolution (Vannucchi et al., 2012). Alkalinity was determined by Gran titration (Gieskes et al., 1991), and sulfate was analyzed using a Dionex ICS-3000 ion chromatograph. Calcium was measured via inductively coupled plasma-atom emission spectrometry (ICP-AES) with a Teledyne Prodigy high-dispersion ICP spectrometer (Murray et al., 2000).

Carbon isotopes of dissolved inorganic carbon (δ^{13}C-DIC) were analyzed at Oregon State University (OSU) after treatment with 100 μL of 43% H_3PO_4 using a Gas Bench II automated sampler interfaced with a Finnigan DELTA plus XL gas source stable isotope mass spectrometer (GS-IRMS; for details see Torres et al., 2005). Based on replicate analyses of a $NaHCO_3$ stock solution, the overall precision of this analysis is better than ±0.15‰.

For isotope analyses of sulfate, filtered pore water aliquots were acidified, and sulfate was precipitated with a 1 M barium chloride solution ($BaCl_2$) to barium sulfate ($BaSO_4$). Sulfur isotope measurements were performed using an EA-IRMS model Delta V (Finnigan; Thermo Fisher Scientific, Waltham, MA, USA) at the University of California, Riverside (UCR). The sulfur isotope data are reported relative to the Vienna Cañon Diablo Troilite (VCDT) standard. The standard deviation (1σ) of replicate measurements of an in-house standard was less than 0.2‰ for δ^{34}S values.

2.3. Solid Phase Analyses

Data for total inorganic carbon (TIC), porosity, and magnetic susceptibility (Ƙ) were collected onboard the DV JOIDES Resolution (Vannucchi et al., 2012). Total inorganic carbon (TIC) was analyzed using a Coulometrics 5011 CO_2 coulometer. Magnetic susceptibility was measured with a Bartington Instruments MS2 meter coupled to a MS2C sensor coil, and porosity was determined by measurement of wet mass, dry mass, and dry volume (Blum, 1997).

Carbonate samples were characterized isotopically at OSU using traditional phosphoric acid digestion and IRMS. Carbonate powders were reacted with 100% phosphoric acid at 75°C, and the isotopic composition was measured using a Kiel III device connected to a Thermo Fisher 252 gas source mass spectrometer. Isotopic analyses with this technique yield a precision better than ± 0.1‰ and 0.2‰ for $\delta^{13}C$ and $\delta^{18}O$, respectively. Instrument calibration was accomplished by comparison to NBS-19. The strontium isotopic composition of the carbonates was determined after a soft-leaching procedure on samples via multi-collector ICP-mass spectrometry (MC-ICP-MS) at OSU. The 2σ errors in the Sr isotope ratios measured by MC-ICP-MS at OSU were ± 0.000028 (for method details see Ruark et al., 2019).

Chromium reducible sulfur (CRS) species were determined using 0.5–1 g frozen wet samples that were treated with a two-step acid Cr (II) distillation method at 200°C for ~2h (Fossing & Jørgensen, 1989) at UCR. Any potential elemental sulfur (S^0) and monosulfides were removed prior to the Cr (II) distillation with methanol followed by a cold ~1h extraction with 6M HCl, collected and characterized via the methylene blue method (because all values of monosulfides and S^0 were below 0.05 wt%, with the majority of the samples below or near the detection limit of ~1 ppm, we did not included these data in our discussion). Once these phases were removed, the released sulfide from CRS was trapped in a 5% w/v Zn-Acetate solution. The trapped CRS samples were sonicated, thoroughly shaken, and an aliquot of each sample was diluted and analyzed spectrophotometrically via the methylene blue method (Cline, 1969). The CRS content data are reported in dry weight percent units. During the Cr (II) reduction step, mainly pyrite and some of greigite are extracted (e.g., Cornwell & Morse, 1987). For simplification, because greigite is typically a minor component, we refer to CRS as pyrite throughout the text. The sulfur isotope composition of CRS ($\delta^{34}S$-CRS) was determined by converting zinc sulfide to silver sulfide (Ag_2S) with a 5% silver nitrate ($AgNO_3$) solution. The precipitate was rinsed and washed with deionized water and 1 M NH_4OH and subsequently dried at approximately 50°C. Sulfur isotope ratios were measured on a EA-IRMS model Delta V as described above for the dissolved sulfate measurements. For further method details see Riedinger et al. (2017).

3. Results and Discussion

We combine the most recent understanding of the subsidence/uplift history of the margin with geochemical information to model the onset of the discrete carbonate layers recovered from Site U1379, which is the shallowest drilled site on this margin.

3.1. Reconstructing Tectonic History of the Margin

By combining drilling results with a large 3-D seismic reflection volume (e.g., Bangs et al., 2015, 2016; Kluesner et al., 2013), Vannucchi et al. (2016) postulated a new framework for the forearc evolution of this margin. Subduction of the main body of the Cocos Ridge led to rapid uplift and subaerial exposure of the forearc, evidenced by shell-rich sandstone typical of beach to nearshore deposition (Figure 2**;** Vannucchi et al., 2012; Harris et al., 2013). The uplift of the margin to or near sea-level is followed by net subsidence caused by erosion at the base of the overriding plate, and the eroded forearc rapidly fills with terrigenous sediment in what Vannucchi et al. (2016) refer to as a depositionary basin. Organic matter degradation within the thick sedimentary package that filled the forearc basin supports active methanogenesis (e.g., Hensen & Wallmann, 2005; Lückge et al., 2002). This revised depositional model also explains the pervasive hydrocarbon venting–a mixture of biogenic and thermogenic source–across the margin (see also Figure 1a; Schmidt et al., 2005; Mau et al., 2006; Kluesner et al., 2013) that could not be supported from the organic carbon present in the thin, mainly pelagic subducting sediment section, where TOC is less than 2.5 wt.%.

The original time frame for the evolution of the forearc offshore the Osa Peninsula was developed on the basis of shipboard biostratigraphic dating (Vannucchi et al., 2013). Post cruise tephrochronology studies yielded a more detailed and revised age model for the margin (Schindlbeck et al., 2016a). In particular, tephra dating at Site U1379, provided a new critical age of 1.4 Ma at 450 m bsf, which differs from the 0.4 Ma age estimate derived from biostratigraphic dating at sea (Schindlbeck et al., 2016a). We use this revised age model in our interpretations (Figures 1c and 2). The more recent stratigraphic ages are in good agreement with model ages from nearby sites (Li et al., 2015).

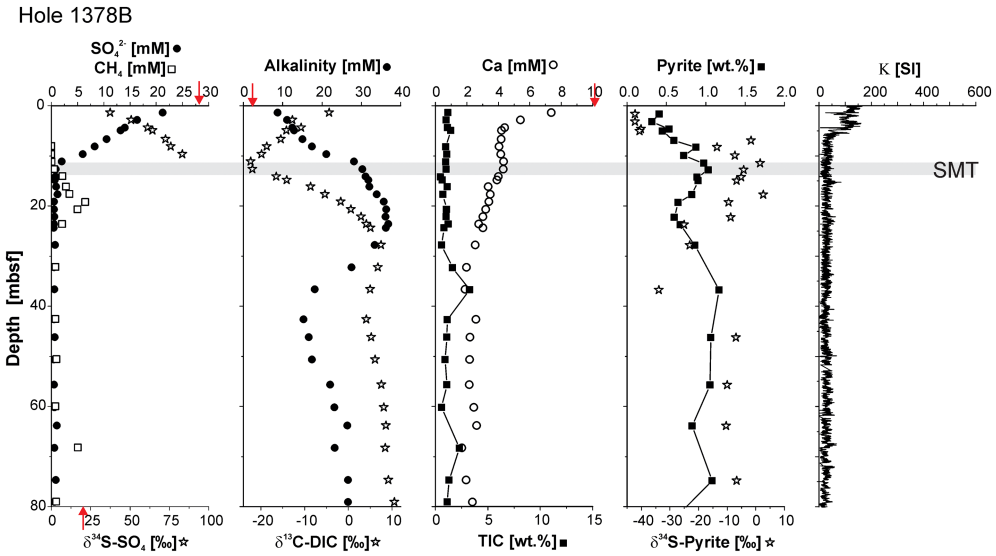

Figure 3. Upper slope Site U1378 pore water concentration profiles of sulfate (SO_4^{2-}) and sulfate sulfur isotopes (δ^{34}S-SO4), alkalinity and dissolved inorganic carbon C-isotopes (δ^{13}C-DIC), and calcium (Ca) as well as solid phase profiles of total inorganic carbon (TIC), pyrite and its sulfur isotopes (δ^{34}S-Pyrite), and the magnetic susceptibility (K). The grey bar displays the sulfate methane transition (SMT). Red arrows indicate average seawater values.

3.2. Contrasting Behavior of Two Sites on the Upper Plate

The main hydrogeologic features of the sites drilled in the context of the CRISP project are described in Vannucchi et al. (2012) and Harris et al. (2013). Here we focus on pore water changes in the upper 50 m bsf at Sites U1378 and U1379 to illustrate recent changes in biogeochemical behavior of two these sites. Although both sites are located on the upper plate, they differ in sedimentological signals and geochemical behavior. Site U1378 shows a steady-state pore water sulfate profile, which decreases linearly with depth from the seafloor to a SMT at around 12 m bsf (Figure 3). The outer shelf Site U1379 is characterized by a concave-down sulfate pore water profile (Figure 4), which, in conjunction with a broad SMT (from 30 to 40 m bsf) and low methane concentrations, indicates a waning of upward methane flow. Deep penetration of seawater sulfate into the sediments, and consequently, a downward shift of the SMT (e.g., Hensen et al., 2003) is characteristic for the end of a venting episode at seep sites (e.g., Roberts & Carney, 1997; Torres et al., 2001).

The result is that magnetic minerals can be buried to greater sediment depth on the upper slope without alteration. This assertion is in agreement with the observation of fine-grained magnetite in sediments below 450 m bsf by Usui et al. (2015). Fine magnetite is typically prone to alteration in sulfide-containing environments. In contrast to Site U1379, the pore water concentration profiles at Site U1378 indicate a steady upward movement of the SMT with sediment burial, leading to production and accumulation of hydrogen sulfide (up to 1.75 mM) at the SMT. Reactive iron oxide minerals, including magnetite, are thus altered into iron sulfide phase expressed in accumulation of ^{34}S-enriched pyrite (up to 1 wt.%). The net result is a decrease in magnetic susceptibility (Figure 3; e.g., Tarduno, 1994; Roberts et al., 1999; Riedinger et al., 2005, 2017; März et al., 2008; Roberts, 2015).

3.3. Carbonate Geochemistry

In addition to pore water profiles indicative of a recent decrease in methane flux, the sediment recovered at Site U1379A contain a sequence of lithified concretions of carbonate mud within Lithologic Unit II (Figure 2). Such distinct layers were not present at Site U1378.

Decades of work on MDAC both along the Costa Rica margin as well as at seeps worldwide have generated a conceptual understanding of how these deposits form (e.g., Aloisi et al., 2000; Naehr et al., 2000; Ritger et al., 1987). The carbonate rich sediment layer at 63 m bsf produced an XRD spectra dominated by calcite, Mg-rich calcite, and aragonite. Carbonate concretions below this layer are predominantly calcite, which is consistent with reports of MDACs worldwide (e.g., Aloisi et al., 2000; Peckmann et al., 2001; Ritger et al., 1987). In

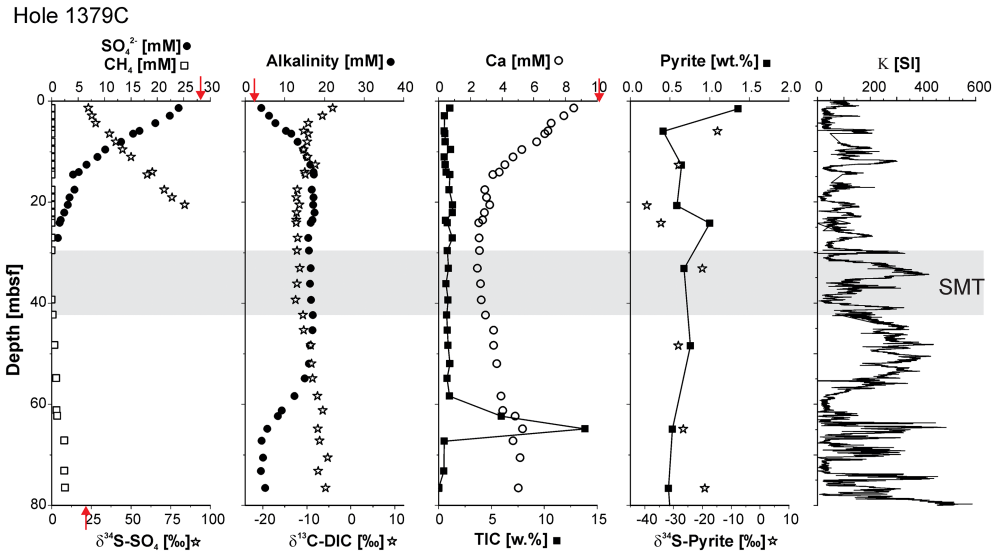

Figure 4. Site U1379 pore water concentration profiles of sulfate (SO42-) and sulfate sulfur isotopes (δ^{34}S-SO4), alkalinity and dissolved inorganic carbon C-isotopes (δ^{13}C-DIC), and calcium (Ca) as well as solid phase profiles of total inorganic carbon (TIC), pyrite and its sulfur isotopes (δ^{34}S-Pyrite), and the magnetic susceptibility (K). The grey bar indicates the sulfate methane transition (SMT). The red arrows indicate average seawater values.

addition, MDACs associated with enhanced methane fluxes at seep sites have been shown to correspond with intervals of magnetic susceptibility (K) drawdowns (e.g., Usapkar et al., 2014). There are two reasons for this observation: (1) formation of authigenic carbonate layers can cause a dilution in the signal of magnetic mineral assemblages and (2) the formation of hydrogen sulfide from AOM can alter iron oxide mineral assemblages and overprint the magnetic signal (e.g., Roberts, 2015, and references therein). At Site U1379, we record slightly higher values of δ^{34}S-pyrite in (and near) some of the carbonate layer intervals (Figure 5), suggesting that the observed drawdowns in magnetic susceptibility in the carbonate-bearing section result from a dynamic system where ferrimagnetic minerals are converted to paramagnetic sulfides during prolonged intervals of AOM. The lack of an absolute correlation of carbonate layers and the depth of K-minima could be attributed to factors such as changes in the primary mineral input; the rate of hydrogen sulfide production and consequently the exposure time of iron minerals to H_2S, and the diagenetic formation of other magnetic minerals such as greigite, an iron sulfide mineral (e.g., Rowan et al., 2009).

The carbon isotope composition of MDAC reflects both the original methane source and the degree of carbon fractionation during AOM (e.g., Gieskes et al., 2005). As illustrated in Figure 6, proximity to the center of gas discharge, as well as the time scale over which the seepage operates, controls the depth of the SMT, AOM rate, and consequently the isotopic composition of the dissolved inorganic carbon (DIC) pool (e.g., Gieskes et al., 2005; Han et al., 2014; Hong et al., 2016, 2018; Teichert et al., 2014). In other words, the closer to the gas discharge center, the higher the methane flux and the more depleted the stable carbon DIC isotope signal (Figure 6). The carbon isotope composition of samples from Site U1379 (Figure 5) are consistent with authigenic deposition at a SMT, where δ^{13}C-DIC has a value of approximately −11‰ (Figures 5 and 6). The isotope signal in the samples is, however, less depleted in δ^{13}C compared to samples collected by Han et al. (2004) from the foci of gas discharge along the upper slope (Figure 6a). The carbon isotope range in Site 1379 samples suggests a methane flux that is lower than those marked by methane advecting rapidly in the gas phase (Figure 6c), such as on a flank of an actively bubbling site similar to reported values by Han et al. (2014; Figure 6b).

The DIC isotopic signal points to low AOM rates consistent with the waning methane flux suggested by the sulfate profile. The δ^{18}O is also lighter than that reported by Han et al. (2014), and only the deepest carbonate sample (~300 m bsf) approaches isotope values similar to those designated as “gas hydrate carbonate” (Han et al., 2014; see also Figure S1 in the supporting information) where hydrate dissociation is responsible for

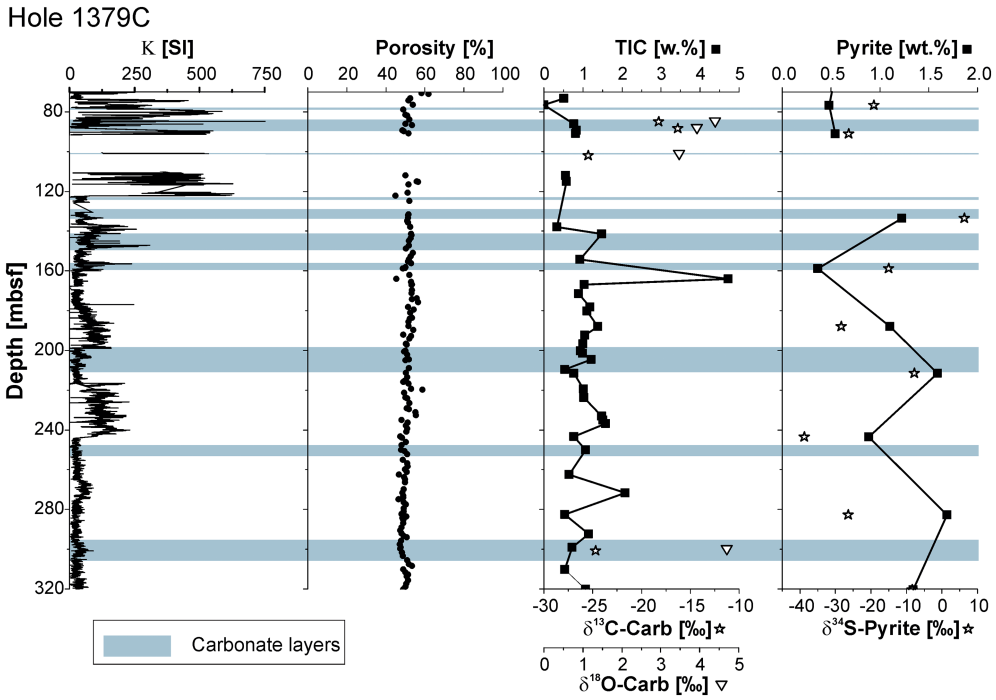

Figure 5. Site U1379 content profiles between 70 and 320 m bsf for the magnetic susceptibility (K), porosity, total inorganic carbon (TIC), pyrite, and its sulfur isotopes (δ^{34}S-Pyrite). The light-blue bars indicate observed carbonate layers (see Vannucchi et al., 2012). It should be noted that most samples for TIC analyses were taken outside observed carbonate layers based on sedimentary description (see also Site U1379 description in Vannucchi et al., 2012).

more positive oxygen isotope values in the pore fluids (Hesse & Harrison, 1981). This possibility agrees with our hypothesis. Specifically, whereas the onset of seepage corresponds to uplift of the margin past the upper edge of hydrate stability, subsequent venting episodes (e.g., Kutterolf et al., 2008) are most likely unrelated to gas hydrate dynamics.

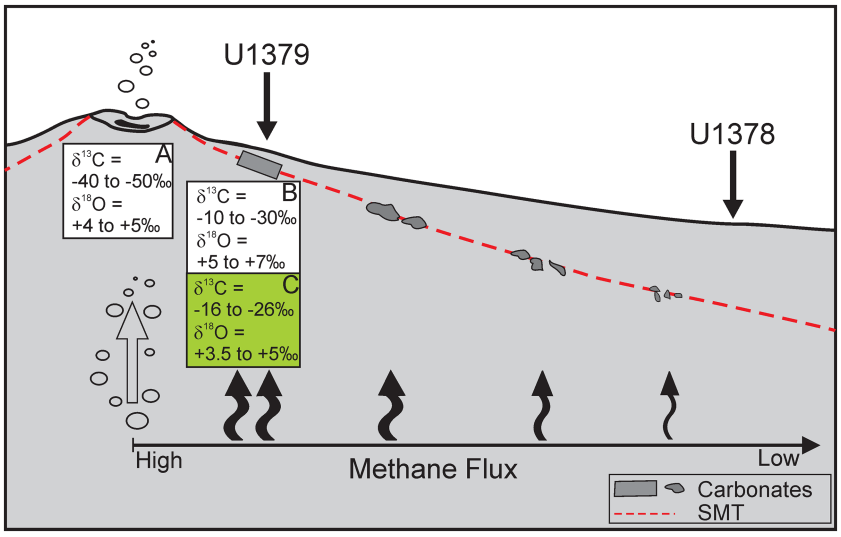

Figure 6. Schematic overview of the suggested paleodepositional environment for Sites U1378 and U1379. The red line marks the sulfate-methane transition (SMT) where carbonates can precipitate related to anaerobic methane oxidation. Open arrow indicates methane gas and black arrows suggest dissolved methane flux. The carbonate stable isotope values of oxygen (δ^{18}O) and carbon (δ^{13}C) in A and B are from Han et al. (2014) for recent, upper slope seep sites off Costa Rica; data in C are from this study.

The $^{87}Sr/^{86}Sr$ ratios in the carbonates, with values between 0.70870 and 0.70911 (Table S5), reflect coeval seawater values within the measurement error, which supports microbial carbon cycling pathways as the main source of alkalinity. The seawater values challenge any potential local impact of silicate weathering reactions that can shift the pore waters away from the Sr-isotope composition of seawater (Sample et al., 2017).

Collectively, the mineralogic and isotopic data of the carbonate sequences recovered at Site U1379 are consistent with formation at a paleo-SMT site. We postulate that the precipitation events reflect past episodes of upward flow of methane-rich fluids, likely on the flanks of gas discharge sites (Figure 6).

3.4. Carbonates as Markers of Venting Episodes

Pore water profiles, including the present isotopic signals of carbon and sulfur at Site U1379, point to a highly dynamic system that has experienced changes in methane flux. These changes can be attributed to various non-steady state processes. Our observations for the sediments from approximately >0.2 Ma, tied to mineral and isotopic composition of the carbonate and decreases in magnetic susceptibility, support the inference that the carbonate layers recovered at this site reflect a series of paleo-episodes of enhanced methane migration.

The eleven layers rich in diagenetic carbonate allow us to explore the episodicity of flow by estimating time and duration of the events. Based on tephra layers at 177 and 375 m bsf, with dates of 0.634 and 1.177 Ma, respectively (Schindlbeck et al., 2016a), we infer that carbonate deposition began ~1.1 Ma. The carbonate layers are ~0.5 to 11 m in thickness. If we use an average sedimentation rate of 300 m/Ma (Figure 2), a first-order approximation for the duration of carbonate deposition is ~1.7 to 37 thousand years (Kyr). Such a period of active venting is too long to correspond to a discrete methane pulse driven by earthquake activity. Furthermore, we would expect a carbonate record spanning longer than 1.1 Myr and extending along the entire margin if seismicity at the fault interface drives methane-derived carbonate precipitation. Our findings are in good agreement, instead, with the episodes of venting previously postulated by Kutterolf et al. (2008), where episodes of fluid venting might have lasted for several tens of thousands of years and could have occurred in multiple cycles at the same venting structure/region.

Here we argue that the onset of carbonate deposition was driven by anaerobic oxidation of a methane pool previously trapped beneath a gas hydrate seal. The fact that gas hydrate act as a permeability barrier for flow has long been postulated and explained by the fact that hydrates occur not as a cement but rather as a load-bearing phase that cuts off pore space connectivity. Whether hydrate can occur as discrete cement or interconnected between pores is still not fully resolved, but recent experiments measuring both hydrate saturation (S_h) and *P*-wave velocity (V_p) under pressure are consistent with a load-bearing hydrate model as presented by Konno et al. (2015). Imaging of methane hydrates using synchrotron X-ray computed microtomography have also shown methane hydrate to form interconnected networks in porous media (Kerkar et al., 2014; Sahoo et al., 2018). In the scenario we postulate, the gas-hydrate permeability seal was breached as Site U1379 uplifted beyond the upper limit of gas hydrate stability, freeing the methane-rich fluids to migrate upward and initiate carbonate precipitation at the SMT.

Whereas a major driver for the onset of venting and associated carbonate deposition at 1.1 Ma can be attributed to methane hydrate destabilization, once the hydrate barrier is breached and Site U1379 continues to shoal above the GHSZ, subsequent methane discharge events are not directly tied to gas hydrate dynamics. Rather, the changes in methane flux responsible for younger carbonate occurrences and for the non-steady state sulfate profile are likely related to episodic venting that is modulated by changes in the underlying methane reservoir. Possible regulators of methane discharge events include changes in methane saturation during margin uplift, periodic charge/release of gas reservoirs, opening of new fluid conduits, and potential self-sealing of migration pathways.

3.5. Gas Hydrate Response to Margin Dynamics

Organic-rich sediments at water depths greater than 300 to 500 m usually host methane hydrates, a solid compound in which methane and other low molecular weight gases are trapped in a water lattice (e.g., Sloan & Koh, 2007). Stability of methane hydrate depends on water pressure and temperature (e.g., Dickens & Quinby-Hunt, 1994):

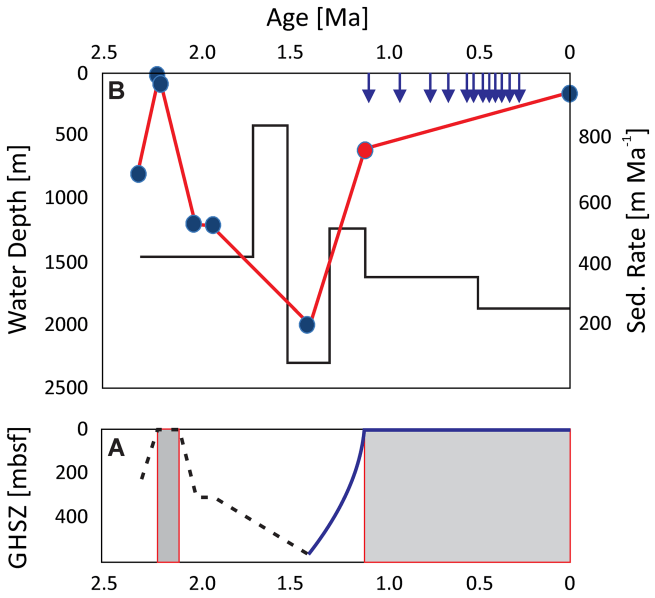

Figure 7. Modeled time frame for (a) the depth of the gas hydrate stability zone (GHSZ) at Site U1379 based on; the grey areas indicate time intervals where the depth was too shallow for gas hydrate formation. (b) an updated tectonic history model (modified after Vannucchi et al., 2016 with new age data from Schindlbeck et al., 2016a). The blue arrows indicate formation of massive authigenic carbonate layers, and red circle demarks onset of authigenic carbonate precipitation as the site reaches at the upper edge of gas hydrate stability shown in panel A.

$$1/(273.15+T) = 3.79{*}10^{-3} - 2.83{\times}10^{-4}(\log P) \quad (1)$$

where T is temperature (°C) at the base of gas hydrate stability (BGHS) and P is water pressure at the BGHS.

We explore our hypothesis that the onset of carbonate deposition at Site U1379 reflects the initiation of methane release driven by changes in methane hydrate stability in response to the uplift and subsidence history of the margin. This exercise can provide a new constraint on the uplift history of the margin. To this end, we use the backstripping results of Vannucchi et al. (2013) to recreate the seafloor depth through time extending back to 2.5 Ma using the new tephra age constraints of Schindlbeck et al., 2016a; Figures 1c and 7a). Paleo-bathymetric inferences are based on sediment and benthic foraminifera that document subsidence, from near or above sea-level about 2.2 Ma to water depths of ~2,000 m bsl at 1.4 Ma (blue circles in Figure 7a). There are no existing data to reconstruct paleo-water depth from 1.4 Ma to the present water depth of 126 m bsl.

We reconstruct the base of gas hydrate stability (BGHS; Figure 7b) since 2.5 Ma using Equation 1 and a thermal gradient of 41.6°C/km based on observations at Site U1379 (Harris et al., 2013; Vannucchi et al., 2012). Past variations in bottom water temperatures and changes in the thermal gradient due to subduction of the Cocos Ridge will alter the estimated BGHS, but the simplification shown here illustrates roughly the impact of uplift and subsidence on gas hydrates stability (Figure 7b). If we then assume that the first appearance of authigenic carbonate at 1.1 Ma corresponds to the time when the BGHS is at the seafloor, we can assign a water depth to this horizon of ~ 600 m bsl. We recognize errors based on the assumption of paleo-bottom water temperatures, but within the margin of error, this new data point provides an additional constrain on the uplift history of the margin, which yields an estimated rate of uplift in the past 1.1 Myr in the order of 400 m/Myr.

3.6. Carbonate Constraints on Uplift and the Volatile Recycling History of the Margin

Our results, when considered in light of the previous work of Vannucchi et al. (2013, 2016) and the new tephrochronology of Schindlbeck et al. (2016a), leads us to the following scenario for margin evolution. The Cocos Ridge initially arrived at the margin 2.91 ±0.23 Ma (Schindlbeck et al., 2016a). Subduction of the main body of the Cocos Ridge at 2.2 ± 0.2 Ma generated a forearc embayment that efficiently trapped terrigenous sediment from the nearby continent and enhanced methane generation. Additional CH_4 was likely supplied from deeper sediments by upward-flow of fluid along the unconformity, as evidenced by geochemical data of Sites U1378 (U1380) and presence of thermogenic hydrocarbons in the 600- to 800-m interval Site U1380 (Harris et al., 2013). In the scenario we propose, the methane pool generated between 2.2 and 1.1 Ma may have been trapped within the sediments either as a gas hydrate or as free gas below a permeability barrier created by gas hydrate growth in interconnected networks that cut off pore space connectivity.

A gas hydrate barrier to upward methane advection is consistent with present-day observations of very limited venting below the edge of gas hydrate stability (Kluesner et al., 2013). This condition would persist as long as the site remained within the GHSZ. At ~1.1 Ma, uplift caused shallowing of the seafloor above the GHSZ (Figure 8). The resulting destabilization allowed upward methane transport, which, upon anaerobic oxidation at the SMT, is transformed into authigenic carbonate. Following 1.1 Ma, Site U1379 remained at depths that were too shallow for gas hydrate formation. As the site continued to shoal, methane continued to be discharged at repeated pulses, some of which were active for prolonged periods (1.7 to 37 thousand years). The longer periods of activity correspond roughly to drawdowns in magnetic susceptibility, consistent with alteration of ferrimagnetic to paramagnetic minerals related to anaerobic methane oxidation (e.g., Riedinger et al., 2005).

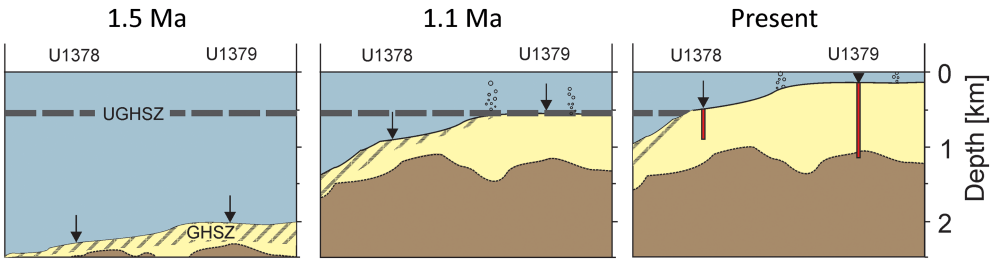

Figure 8. Simplified sketch of time slices for the last 1.5 million years with regard to the gas hydrate stability zone (GHSZ) at the investigated sites based on the updated tectonic history (Figure 7). The dashed area depicts the GHSZ and dashed line indicates the upper limit for gas hydrate stability (upper gas hydrate stability zone, UGHSZ).

Episodic methane discharge, a process we postulate for Site U1379, was recognized as the driving force for the formation of large forearc carbonate mound structures offshore Nicaragua and Costa Rica (Kutterolf et al., 2008). These authors documented highly active periods of venting that lasted 10–50 thousand years, with intervening inactive periods that spanned more than 10 thousand years. This, and other instances of episodic methane discharge described elsewhere (e.g., Teichert et al., 2003; Leon et al., 2007; Cremiere et al., 2016; Hong et al., 2017; Loher et al., 2018), have been attributed to a variety of forcing mechanisms that include localized conditions at a given fault (changes in local high permeability pathways), fluctuations in the methane reservoir (charge/recharge episodes), regional tectonics (methane release due to uplift and/or fault generation), and changes in eustatic sea level. A combination of these factors was likely at play at Site U1379, where the episodicity recorded in carbonate deposits following the initial methane pulse reveal forcing mechanisms that are not directly tied to gas hydrate changes at the site, which was above the GHSZ after 1.1 Ma (Figure 7a).

Methane seepage and MDAC precipitation since this site shoaled above the upper limit of gas hydrate stability fits with the regional picture of pervasive methane discharge that was documented at other sites located at or above the upper edge of gas hydrate stability. These sites are identified through high-backscatter anomalies, bathymetric expressions, and hydroacoustic data (e.g., Kluesner et al., 2013). Geophysics data from this margin and elsewhere clearly show that location of migration paths (e.g. faults) plays a dominant role in how much methane reaches a site and determines the well-defined discrete sites of methane expulsion. Although margins are punctuated by seepage sites, even in highly dense seep patches such as those mapped in the upper slope and shelf region offshore the Osa Peninsula (Figure 1a), there are significant areas of the seafloor with no indication of methane discharge, no chemosynthetic communities, and no authigenic carbonate. It was rather fortunate that coring at Site U1379 pierced a clear and long-lived focus of methane release.

The extreme dynamic environment at Site U1379 contrasts with the record recovered at Sites U1378 and the companion Site U1380 (Figure 1). The presence of a shell-rich sand to sandstone unit, which is also present at the unconformity at Site U1380, is indicative of shallower water depth, which was followed by rapid subsidence and rapid deposition of land-derived volcanogenic turbidites in the fore-arc basin. However, the material recovered at Site U1378 is mostly re-sedimented from shallower water and not deposited in situ —in contrast to Site U1379. Additionally, the upper slope site remained within the zone of gas hydrate stability, and it is not until very recently that it reached the 600 m water depth that represents the upper limit of gas hydrate stability zone along this margin. The pore water profiles at Site U1378 reflect a steady state condition, with no evidence of recent changes in methane flux (Figure 3). It is possible that any accumulated methane-bearing fluid beneath the gas hydrate stability zone at Sites U1378/U1380 may have migrated toward the shallower shelf region where methane discharge occurred in settings analogous to U1379. Additionally, the occurrences of fluid migration pathways, such as fault structures (Fig**ure 1b**), are known to impact the amount of methane that potentially reaches a specific site.

3.7. Interpretation of Our Results in the Context of Seismic Evidence for Venting

The sites discussed here were drilled along a transect immediately to the south of the 3-D -seismic volume described in Kluesner et al. (2013). Site U1413 was drilled in 540 of water within the region covered by this survey (Figure 1a). Although we do not have a complete data set for Site U1413 comparable to what we

presented for Sites U1378 and U1379, we note that, similar to the situation at Site U1378 (at 533 m bsl), no MDACs were recovered at U1413. The reasons for the lack of MDACs at U1413 are therefore likely similar to those presented for U1378. U1413 is currently close to the edge of hydrate stability where seismic data show lower prevalence of seep sites (Figure 1). Thus, any gas released as the margin shoaled likely migrated to shallower regions, and the lower density of gas vents at the 500–600 m bsf band are likely tied to migration pathways not pierced by drilling.

In agreement with the hypothesis of Sahling et al. (2008), Kluesner et al. (2013) attributed seepage in this region of the margin to the effects of seamount and/or ridge subduction. Seismic acoustic evidence of gas pockets present under many of the seeps, as well as evidence of buried paleo-seepage sites, was interpreted to result from episodic methane venting driven by gas reservoir dynamics so that when gas accumulation was sufficiently overpressured to breach the sediment trap, gas leaked and vented at the seafloor (Kluesner et al., 2013). These geophysical inferences are in agreement with the conceptual model we propose based on drilling data. We expand the geophysical interpretations by providing geochemical evidence for episodic methane pulses in the shelf region, which is undoubtedly tied to changes in the margin hydrology in response to ridge subduction. We further show that in addition to fault generation, the uplift and subsidence response of the margin to the subduction of the Cocos Ridge impacted the gas hydrate stability field, and this long-term perturbation further modulated the volatile recycling history of the margin.

3.8. Importance for the Ancient Rock Record

The occurrence of massive carbonate layers within the sediments and their association to changes in methane flux related to gas hydrate dynamics and/or methane flow pathways might be used to understand the occurrence of massive carbonate concretions observed in the ancient rock record. Discrete diagenetic beds or laterally continuous horizons of ellipsoidal concretions have been observed in several ancient shale formations (e.g., Raiswell, 1971; Coleman & Raiswell, 1981; Kirkland et al., 1992; Coleman, 1993). Although these carbonate concretions have been extensively analyzed, especially for their oxygen and carbon isotope signatures to potentially infer paleo-temperature and formation timing (see compilation in: Mozley & Burns, 1993), the formation process itself that led to the massive carbonate deposits and why/how the concretions are preserved within the host sediments over long periods of time remains a mystery.

Recently, Lash (2015) suggested that carbonate concretions observed in Upper Devonian Hanover shale deposits near west of New York might have formed near the sediment surface at the SMT due to pulses of high methane fluxes (and with that higher AOM rates). These observed carbonate concretions are embedded in clastic material comprising mainly of silt and clay with high organic content (Lash & Blood, 2004). Similar carbonate concretions were discovered in organic-rich Devonian Woodford shales (Kirkland et al., 1992). The Woodford Shale concretions revealed a carbonate $\delta^{13}C$ signal in the concretion center of −15 to −18‰ (Martin, 2017). These carbonate $\delta^{13}C$ values are very similar to those observed in the carbonate layers from our study area. All these reported massive carbonate concretions have in common that they overlie hydrocarbon producing material. The production of methane (and other hydrocarbons) likely resulted in varying methane flux over time depending on burial rates that were influenced by tectonic processes and variation in sedimentation rates (e.g., Lash & Blood, 2004). We therefore suggest that tectonically induced methane venting events that potentially resulted in the formation of the eleven carbonate mud sequences within the sediments at Site U1379 might provide a “modern” analogue for the formation of carbonate concretions observed in ancient rock formations.

4. 5 Summary and Conclusions

As the upper plate began to uplift ~1.4 Ma, following subduction of the Cocos Ridge offshore of the Osa Peninsula off Costa Rica, the sediment package currently in the outer shelf shoaled above the gas hydrate stability field by ~1.1 Ma. This process resulted in a sudden upward methane flux driven by gas hydrate destabilization and migration of gas previously trapped beneath the gas hydrates. We postulate that the onset of authigenic carbonate sequences recovered by drilling at IODP Site U1379 marks the uplift out of the GHSZ. Under this assumption, our results provide additional constraints on the uplift history and a new estimate of uplift rate of ~400 m in the last 1 million years. As the sediment continued to shoal, methane was free to vent in sediments above the GHSZ, leading to the high density of seepage sites now known to occur in the outer shelf region (Kluesner et al., 2013). Methane discharge in this region is highly episodic, as has been

shown by analyses of carbonate mounds in this region (Kutterolf et al., 2008). Venting episodicity may have been modulated by periodic charge/release cycles from gas reservoirs that could have been affected by methane saturation changes during margin uplift. The episodicity of methane discharge in the outer shelf is revealed at Site U1379 by discrete carbonate layers as young as 0.63 Ma and by non-steady state pore water profiles indicative of a recent waning of methane pulses.

The observed geochemical signals reveal fluid release events in response to uplift and subsidence episodes associated with the Cocos Ridge subduction offshore the Osa Peninsula, with relevance to volatile recycling budgets. Using data collected at seep sites in the northern Costa Rica margin, Füri et al. (2010) concluded that the carbon released via submarine fluid venting at the outer forearc is less than 1% of the carbon input to the subduction zone and the output at the volcanic front. More recently, Barry et al. (2019) suggested that this carbon deficit can be resolved by incorporating the carbon sequestered as carbonate in the forearc in the budgets. These authors used helium and carbon isotope data from deep sourced fluids to estimate that ~91% of the forearc carbon is sequestered as calcite and that methane emissions contribute negligibly to the total carbon budget in the forearc. We agree that sequestration as carbonate minerals likely contributes significantly to the overall carbon inventories, but the analysis by Barry et al. (2019) did not include the carbon input from terrestrial material that rapidly filled the forearc basin following the subduction of the Cocos Ridge. The rapid burial of the sediments resulted in significant methane formation and accumulation in the margin wedge as documented by scientific drilling (Harris et al., 2013; Kimura et al., 1997; Vannucchi et al., 2012). The results presented here for Site U1379 illustrate how tectonic uplift processes in this margin allowed methane to migrate towards the SMT, where the increase in alkalinity driven by the anaerobic methane oxidation led to carbon sequestration as MDAC. These carbonates are consistent with the widespread gas seepage and carbonate deposition at, and shallower than, the upper edge of gas hydrate stability inferred from geophysical data (e.g., Kluesner et al., 2013). The arcuate shape of the shelf edge, the projection of the Quepos Ridge, and the high density of potential seep sites suggest that this area may be a zone of former seamount/ridge subduction. If true, the processes described at Site U1379 may have been active over geologic time scales. Our integrated approach provides new insights into forearc volatile recycling in response to subduction of the Cocos Ridge beneath the Caribbean plate.

Acknowledgments
We thank the officers and crew as well as the drilling personnel and the scientific parties of IODP Expedition 334 and 344. This research used samples and data provided by the IODP, which is sponsored by the U.S. National Science Foundation and participating countries and universities under management of IODP Management International, Inc. All data analyzed on board the D/V Joides Resolution during expedition IODP 334 are available via the IODP database LIMS. All other data are available in the supplemental material and archived in the World Data Center PANGAEA. This is an Oklahoma State University-Boone Pickens School of Geology contribution 2019-106. The research was funded by USSSP post-expedition (Expedition 334) awards T334B11 to Marta Torres and T344A28 to Elizabeth Screaton. Steffen Kutterolf kindly thanks the German Research Foundation for funding CRISP related research (Ku-2685/2-1&2). We are indebted to S. Bates and E. Goldbaum for their assistance in the lab and two anonymous reviewers are thanked for their valuable input, which improved the quality and clarity of this manuscript. Marta Torres and Natascha Riedinger gratefully acknowledge a fellowship of the Hanse-Wissenschaftskolleg (HWK, Institute for Advanced Studies), Delmenhorst, Germany, and Natascha Riedinger gratefully acknowledges the Shelia Seaman Writing Retreat: for women geoscientists. The authors declare that the research was conducted in the absence of any commercial or financial relationships that could be construed as a potential conflict of interest.

References

Aloisi, G., Pierre, C., Rouchy, J. M., Foucher, J. P., & Woodside, J. (2000). Methane-related authigenic carbonates of eastern Mediterranean Sea mud volcanoes and their possible relation to gas hydrate destabilisation. *Earth and Planetary Science Letters*, *184*(1), 321–338.

Bangs, N. L., McIntosh, K. D., Silver, E. A., Kluesner, J. W., & Ranero, C. R. (2015). Fluid accumulation along the Costa Rica subduction thrust and development of the seismogenic zone. J. Geophys. Res. *Solid Earth*, *120*, 67–86. https://doi.org/10.1002/2014JB011265

Bangs, N. L., McIntosh, K. D., Silver, E. A., Kluesner, J. W., & Ranero, C. R. (2016). A recent phase of accretion along the southern Costa Rican subduction zone. *Earth and Planetary Science Letters*, *443*, 204–215.

Barry, P.H., de Moor, J.M., Giovannelli, D., Schrenk, M., Hummer, D.R., Lopez, T., et al. (2019). Forearc carbon sink reduces long-term volatile recycling into the mantle. Nature, 568(7753), p.487.

Blum, P. (1997). Physical properties handbook: A guide to the shipboard measurement of physical properties of deep-sea cores. *College Station, TX: Ocean Drilling Program*; Ocean Drilling Project Technical Note.

Bohrmann, G., Heeschen, K., Jung, C., Weinrebe, W., Baranov, B., Cailleau, B., et al. (2002). Widespread fluid expulsion along the seafloor of the Costa Rica convergent margin. *Terra Nova*, *14*(2), 69–79.

Borowski, W. S., Paull, C. K., & Ussler, W. III (1999). Global and local variations of interstitial sulfate gradients in deep-water, continental margin sediments: Sensitivity to underlying methane and gas hydrates. *Marine Geology*, *159*(1-4), 131–154.

Cline, J. D. (1969). Spectrophotometric determination of hydrogen sulfide in natural waters. *Limnology and Oceanography*, *14*, 454–458. https://doi.org/10.4319/lo.1969.14.3.0454

Coleman, M. L. (1993). Microbial processes: Controls on the shape and composition of carbonate concretions. *Marine Geology*, *113*(1-2), 127–140.

Coleman, M. L., & Raiswell, R. (1981). Carbon, oxygen and sulphur isotope variations in concretions from the Upper Lias of NE England. *Geochimica et Cosmochimica Acta*, *45*(3), 329–340.

Cornwell, J. C., & Morse, J. W. (1987). The characterization of iron sulfide minerals in anoxic marine sediments. *Marine Chemistry*, *22*, 193–206. https://doi.org/10.1016/0304-4203(87)90008-9

Crémière, A., Lepland, A., Chand, S., Sahy, D., Condon, D.J., Noble, S.R., et al. (2016). Timescales of methane seepage on the Norwegian margin following collapse of the Scandinavian Ice Sheet. Nature Comm.s, 7, p.11509.

Dewangan, P., Basavaiah, N., Badesab, F. K., Usapkar, A., Mazumdar, A., Joshi, R., & Ramprasad, T. (2013). Diagenesis of magnetic minerals in a gas hydrate/cold seep environment off the Krishna–Godavari basin, Bay of Bengal. *Marine Geology*, *340*, 57–70.

Dickens, G. R., & Quinby-Hunt, M. S. (1994). Methane hydrate stability in seawater. *Geophysical Research Letters*, *21*, 2115–2118. https://doi.org/10.1029/94GL01858

Egger, M., Riedinger, N., Mogollón, J. M., and Jørgensen, B. B. (2018). Global diffusive fluxes of methane in marine sediments. Nature Geosci., 11(6), 421.

Evrenos, A. I., Heathman, J. K., & Ralstin, J. (1971). Impermeation of porous media by forming hydrates in situ. *Journal of Petroleum Technology*, *23*(09), 1–059.

Expedition 334 Scientists (2012). *Site U1381. In Vannucchi, P., Ujiie, K., Stroncik, N., and the Expedition 334 Scientists, Proc. IODP, 334.* Tokyo: Integrated Ocean Drilling Program Management International, Inc. https://doi.org/10.2204/iodp.proc.334.106.2012

Fossing, H., & Jørgensen, B. B. (1989). Measurement of bacterial sulfate reduction in sediments. *Evaluation of a single-step chromium reduction method. Biogeochemistry*, *8*, 205–222. https://doi.org/10.1007/BF00002889

Füri, E., Hilton, D. R., Tryon, M. D., Brown, K. M., McMurtry, G. M., Brückmann, W., & Wheat, C. G. (2010). Carbon release from submarine seeps at the Costa Rica fore arc: Implications for the volatile cycle at the Central America convergent margin. *Geochemistry, Geophysics, Geosystems*, *11*, Q04S21. https://doi.org/10.1029/2009GC002810

Gieskes, J., Mahn, C., Day, S., Martin, J. B., Greinert, J., Rathburn, T., & McAdoo, B. (2005). A study of the chemistry of pore fluids and authigenic carbonates in methane seep environments: Kodiak Trench, Hydrate Ridge, Monterey Bay, and Eel River Basin. *Chemical Geology*, *220*(3-4), 329–345.

Gieskes, J. M., Gamo, T., & Brumsack, H. (1991). Chemical methods for interstitial water analysis aboard JOIDES Resolution. *ODP Tech. Note*, *15*. https://doi.org/10.2973/odp.tn.15.1991

Han, X., Suess, E., Liebetrau, V., Eisenhauer, A., & Huang, Y. (2014). Past methane release events and environmental conditions at the upper continental slope of the South China Sea: Constraints by seep carbonates. *International Journal of Earth Sciences*, *103*(7), 1873–1887.

Harris, R. N., Sakaguchi, A., Petronotis, K., & the Expedition 344 Scientists (2013). *Proceeding IODP, Volume 344.* College Station, TX: Integrated Ocean Drilling Program.

Hensen, C., & Wallmann, K. (2005). Methane formation at Costa Rica continental margin—constraints for gas hydrate inventories and cross-décollement fluid flow. *Earth and Planetary Science Letters*, *236*(1-2), 41–60.

Hensen, C., Zabel, M., Pfeifer, K., Schwenk, T., Kasten, S., Riedinger, N., et al. (2003). Control of sulfate pore-water profiles by sedimentary events and the significance of anaerobic oxidation of methane for burial of sulfur in marine sediments. *Geochimica et Cosmochimica Acta*, *67*, 2631–2647. https://doi.org/10.1016/s0016-7037(03)00199-6

Hesse, R., & Harrison, W. E. (1981). Gas hydrates (clathrates) causing pore-water freshening and oxygen isotope fractionation in deep-water sedimentary sections of terrigenous continental margins. *Earth and Planetary Science Letters*, *55*(3), 453–462.

Hong, W. L., Sauer, S., Panieri, G., Ambrose, W. G., James, R. H., Plaza-Faverola, A., & Schneider, A. (2016). Removal of methane through hydrological, microbial, and geochemical processes in the shallow sediments of pockmarks along eastern Vestnesa Ridge (Svalbard). *Limnology and Oceanography*, *61*(S1).

Hong, W. L., Torres, M. E., Carroll, J., Crémiere, A., Panieri, G., Yao, H., & Serov, P. (2017). Seepage from an arctic shallow marine gas hydrate reservoir is insensitive to momentary ocean warming. *Nature Communications*, *8*, 15745.

Hong, W. L., Torres, M. E., Portnov, A., Waage, M., Haley, B., & Lepland, A. (2018). Variations in gas and water pulses at an Arctic seep: Fluid sources and methane transport. *Geophysical Research Letters*, *45*(9), 4153–4162.

Joseph, C., Campbell, K. A., Torres, M. E., Martin, R. A., Pohlman, J. W., Riedel, M., & Rose, K. (2013). Methane-derived authigenic carbonates from modern and paleoseeps on the Cascadia margin: Mechanisms of formation and diagenetic signals. *Palaeogeography Palaeoclimatology Palaeoecology*, *390*, 52–67.

Karlin, R., & Levi, S. (1983). Diagenesis of magnetic minerals in recent hemipelagic sediments. *Nature*, *303*(5915), 327–330. https://doi.org/10.1038/303327a0

Kerkar, P. B., Horvat, K., Jones, K. W., and Mahajan, D. (2014). Imaging methane hydrates growth dynamics in porous media using synchrotron X-ray computed microtomography. *Geochemistry, Geophysics, Geosystems*, *15*, 4759-4768. https://doi.org/10.1002/2014gc005373

Kimura, G., Silver, E. A., Blum, P., et al. (1997). *Proceedings of the Ocean Drilling Program, Initial reports, Volume 170: College Station*, (p. 458). Texas: Ocean Drilling Program.

Kirkland, D. W., Denison, R. E., Summers, D. M.,Gormly, J. R.,Johnson, K. S. & Cardott, B. J. (1992). Geology and organic geochemistry of the Woodford Shale in the Criner Hills and Western Arbuckle Mountains Oklahoma, in. In K. S. Johnson, & B. J. Cardott (Eds.), *Source Rocks in the Southern Midcontinent 1990 Symposium*, (Vol. 93, pp. 38–69). Oklahoma: Geological Survey Circular.

Kluesner, J. W., Silver, E. A., Gibson, J., Bangs, N. L., McIntosh, K. D., Orange, D., et al. (2013). High density of structurally controlled, shallow to deep water fluid seep indicators imaged offshore Costa Rica. *Geochemistry, Geophysics, Geosystems*, *14*, 519–539. https://doi.org/10.1002/ggge.20058

Konno, Y., Jin, Y., Yoneda, J., Kida, M., Egawa, K., Ito, T., et al. (2015). Effect of methane hydrate morphology on compressional wave velocity of sandy sediments: Analysis of pressure cores obtained in the Eastern Nankai Trough. *Marine and Petroleum Geology*, *66*, 425–433.

Kutterolf, S., Liebetrau, V., Mörz, T., Freundt, A., Hammerich, T., & Garbe-Schönberg, D. (2008). Lifetime and cyclicity of fluid venting at forearc mound structures determined by tephrostratigraphy and radiometric dating of authigenic carbonates. *Geology*, *36*(9), 707–710. https://doi.org/10.1130/G24806A.1

LaFemina, P., Dixon, T. H., Govers, R., Norabuena, E., Turner, H., Saballos, A., et al. (2009). Fore-arc motion and Cocos Ridge collision in Central America. *Geochemistry, Geophysics, Geosystems*, *10*, Q05S14. https://doi.org/10.1029/2008GC002181

Lash, G. G. (2015). Authigenic barite nodules and carbonate concretions in the Upper Devonian shale succession of western New York–a record of variable methane flux during burial. *Marine and Petroleum Geology*, *59*, 305–319.

Lash, G. G., & Blood, D. (2004). Geochemical and textural evidence for early (shallow) diagenetic growth of stratigraphically confined carbonate concretions, Upper Devonian Rhinestreet black shale, western New York. *Chemical Geology*, *206*(3-4), 407–424.

Li, Y. X., Zhao, X., Jovane, L., Petronotis, K. E., Gong, Z., & Xie, S. (2015). Paleomagnetic constraints on the tectonic evolution of the Costa Rican subduction zone: New results from sedimentary successions of IODP drill sites from the Cocos Ridge. *Geochemistry, Geophysics, Geosystems*, *16*, 4479–4493. https://doi.org/10.1002/2015GC006058

Loher, M., Marcon, Y., Pape, T., Römer, M., Wintersteller, P., dos Santos Ferreira, C., et al. (2018). Seafloor sealing, doming, and collapse associated with gas seeps and authigenic carbonate structures at Venere mud volcano, Central Mediterranean. *Deep Sea Research Part I: Oceanographic Research Papers*, *137*, 76–96.

Lückge, A., Kastner, M., Littke, R., & Cramer, B. (2002). Hydrocarbon gas in the Costa Rica subduction zone: Primary composition and post-genetic alteration. *Organic Geochemistry*, *33*(8), 933–943.

Martin, D. P. (2017). Geologic Characterization of Enigmatic Carbonate Masses in the Woodford Shale in *Criner Hills Area, Oklahoma*. Oklahoma State University: Master Thesis.https://hdl.handle.net/11244/300032

März, C., Hoffmann, J., Bleil, U., de Lange, G. J., & Kasten, S. (2008). Diagenetic changes of magnetic and geochemical signals by anaerobic methane oxidation in sediments of the Zambezi deep-sea fan (SW Indian Ocean). *Marine Geology*, *255*, 118–130. https://doi.org/10.1016/j.margeo.2008.05.013

Mau, S., Rehder, G., Arroyo, I. G., Gossler, J., & Suess, E. (2007). Indications of a link between seismotectonics and CH4 release from seeps off Costa Rica. *Geochemistry, Geophysics, Geosystems*, *8*, Q04003. https://doi.org/10.1029/2006GC001326

Mau, S., Sahling, H., Rehder, G., Suess, E., Linke, P., & Söding, E. (2006). Estimates of methane output from mud extrusions at the erosive convergent margin off Costa Rica. *Marine Geology*, *225*(1-4), 129–144.

Moerz, T., Kopf, A., Brueckmann, W., Sahling, H., Fekete, N., Hühnerbach, V., et al. (2005). *Styles and productivity of diapirism along the Middle America margin, part I: Margin evolution, segmentation, dewatering and mud diapirism, in Martinelli, G., and Panahi, B., eds., Mud volcanoes, geodynamics and seismicity*, (pp. 35–48). Dordrecht, Springer: NATO Science Series.

Mozley, P. S., & Burns, S. J. (1993). Oxygen and carbon isotopic composition of marine carbonate concretions; an overview. *Journal of Sedimentary Research*, *63*(1), 73–83.

Murray, R.W., Miller, D.J., and Kryc, K.A. (2000). Analysis of major and trace elements in rocks, sediments, and interstitial waters by inductively coupled plasma–atomic emission spectrometry (ICP-AES). *ODP Tech*. Note, *29*. https://doi.org/10.2973/odp.tn.29.2000

Naehr, T.H., Rodriguez, N.M., Bohrmann, G., Paull, C.K. and Botz, R. (2000). 29. Methanederived authigenic carbonates associated with gas hydrate decomposition and fluid venting above the Blake Ridge Diapir. *In Proceedings of the Ocean Drilling Program, Scientific Results* (Vol. *164*, pp. 285-300).

Neretin, L. N., Böttcher, M. E., Jørgensen, B. B., Volkov, I. I., Lüschen, H., & Hilgenfeldt, K. (2004). Pyritization processes and greigite formation in the advancing sulfidization front in the Upper Pleistocene sediments of the Black Sea. *Geochimica et Cosmochimica Acta*, *68*(9), 2081–2093.

Niewöhner, C., Hensen, C., Kasten, S., Zabel, M., & Schulz, H. D. (1998). Deep sulfate reduction completely mediated by anaerobic methane oxidation in sediments of the upwelling area off Namibia. *Geochimica et Cosmochimica Acta*, *62*(3), 455–464.

Peckmann, J., Reimer, A., Luth, U., Luth, C., Hansen, B. T., Heinicke, C., et al. (2001). Methane-derived carbonates and authigenic pyrite from the northwestern Black Sea. *Marine Geology*, *177*(1-2), 129–150.

Pierre, C., Blanc-Valleron, M. M., Demange, J., Boudouma, O., Foucher, J. P., Pape, T., et al. (2012). Authigenic carbonates from active methane seeps offshore southwest Africa. *Geo-Marine Letters*, *32*(5-6), 501–513.

Raiswell, R. (1971). The growth of Cambrian and Liassic concretions. *Sedimentology*, *17*(3-4), 147–171.

Ranero, C.R., Grevemeyer, I., Sahling, U., Barckhausen, U., Hensen, C., Wallmann, K., Weinrebe,W., et al. (2008). The hydrogeological system of erosional convergent margins and its influence on tectonics and interpolate seismogenesis. Geochem., *Geophys., Geosyst*. *9*, Q03. https://doi.org/10.1029/2007GC001679.

Ranero, C. R., & von Huene, R. (2000). Subduction erosion along the Middle America convergent margin. *Nature*, *404*(6779), 748.

Reeburgh, W. S. (2007). Oceanic methane biogeochemistry. *Chemical Reviews*, *107*(2), 486–513.

Riedel, M., Novosel, I., Spence, G. D., Hyndman, R. D., Chapman, R. N., Solem, R. C., & Lewis, T. (2006). Geophysical and geochemical signatures associated with gas hydrate–related venting in the northern Cascadia margin. *Geological Society of America Bulletin*, *118*(1-2), 23–38.

Riedinger, N., Brunner, B., Krastel, S., Arnold, G. L., Wehrmann, L. M., Formolo, M. J., et al. (2017). Sulfur cycling in an iron oxide-dominated, dynamic marine depositional system: The Argentine continental margin. *Frontiers in Earth Science*, *5*, 33.

Riedinger, N., Pfeifer, K., Kasten, S., Garming, J. F. L., Vogt, C., & Hensen, C. (2005). Diagenetic alteration of magnetic signals by anaerobic oxidation of methane related to a change in sedimentation rate. *Geochimica et Cosmochimica Acta*, *69*, 4117–4126. https://doi.org/10.1016/j.gca.2005.02.004

Ritger, S., Carson, B., & Suess, E. (1987). Methane-derived authigenic carbonates formed by subduction-induced pore-water expulsion along the Oregon/Washington margin. *Geological Society of America Bulletin*, *98*(2), 147–156.

Roberts, A. P. (2015). Magnetic mineral diagenesis. *Earth-Science Reviews*, *151*, 1–47.

Roberts, A. P., Stoner, J. S., & Richter, C. (1999). Diagenetic magnetic enhancement of sapropels from the eastern Mediterranean Sea. *Marine Geology*, *153*(1-4), 103–116.

Roberts, H. H., & Carney, R. S. (1997). Evidence of episodic fluid, gas, and sediment venting on the northern Gulf of Mexico continental slope. *Economic Geology*, *92*(7-8), 863–879.

Rowan, C. J., Roberts, A. P., & Broadbent, T. (2009). Reductive diagenesis, magnetite dissolution, greigite growth and paleomagnetic smoothing in marine sediments: A new view. *Earth and Planetary Science Letters*, *277*(1–2), 223–235. https://doi.org/10.1016/j.epsl.2008.10.016

Ruark, C., Torres, M.E., Muratli, J., and Solomon, E.A. (2019). Data report: Isotopic and elemental analyses of pore fluids and carbonates from Sites U1378 and U1380 drilled during CRISP-A Expeditions 334 and 344 in the middle slope offshore Costa Rica. In Harris, R.N., Sakaguchi, A., Petronotis, K., and the Expedition 344 Scientists, Proceedings of the Integrated Ocean Drilling Program, 344: College Station, TX (Integrated Ocean Drilling Program). https://doi.org/10.2204/iodp.proc.344.208.2019

Sahling, H., Masson, D. G., Ranero, C. R., Hühnerbach, V., Weinrebe, W., Klaucke, I., et al. (2008). Fluid seepage at the continental margin offshore Costa Rica and southern Nicaragua. *Geochemistry, Geophysics, Geosystems*, *9*, Q05S05. https://doi.org/10.1029/2008GC001978

Sahoo, S. K., Madhusudhan, B. N., Marín-Moreno, H., North, L. J., Ahmed, S., Falcon-Suarez, I. H., et al. (2018). Laboratory Insights Into the Effect of Sediment-Hosted Methane Hydrate Morphology on Elastic Wave Velocity From Time-Lapse 4-D Synchrotron X-Ray Computed Tomography. *Geochemistry, Geophysics, Geosystems*, *19*(11), 4502–4521.

Sample, J. C., Torres, M. E., Fisher, A., Hong, W. L., Destrigneville, C., Defliese, W. F., & Tripati, A. E. (2017). Geochemical constraints on the temperature and timing of carbonate formation and lithification in the Nankai Trough. *NanTroSEIZE transect. Geochim. Cosmochim. Acta*, *198*, 92–114.

Schindlbeck, J. C., Kutterolf, S., Freundt, A., Straub, S. M., Vannucchi, P., & Alvarado, G. E. (2016a). Late Cenozoic tephrostratigraphy offshore the southern Central American Volcanic Arc: 2. Implications for magma production rates and subduction erosion. *Geochemistry, Geophysics, Geosystems*, *17*, 4585–4604. https://doi.org/10.1002/2016GC006504

Schmidt, M., Hensen, C., Mörz, T., Müller, C., Grevemeyer, I., Wallmann, K., et al. (2005). Methane hydrate accumulation in "Mound 11" mud volcano, Costa Rica forearc. *Marine Geology*, *216*(1-2), 83–100.

Sloan, E. D. Jr., & Koh, C. (2007). *Clathrate hydrates of natural gases*. CRC press.

Tarduno, J. A. (1994). Temporal trends of magnetic dissolution in the pelagic realm: Gauging paleoproductivity? *Earth and Planetary Science Letters*, *123*(1–3), 39–48. https://doi.org/10.1016/0012-821X(94)90255-0

Teichert, B. M. A., Eisenhauer, A., Bohrmann, G., Haase-Schramm, A., Bock, B., & Linke, P. (2003). U/Th systematics and ages of authigenic carbonates from Hydrate Ridge, Cascadia Margin: Recorders of fluid flow variations. *Geochimica et Cosmochimica Acta*, *67*(20), 3845–3857.

Teichert, B. M. A., Johnson, J. E., Solomon, E. A., Giosan, L., Rose, K., Kocherla, M., et al. (2014). Composition and origin of authigenic carbonates in the Krishna–Godavari and Mahanadi Basins, eastern continental margin of India. *Marine and Petroleum Geology*, *58*, 438–460.

Torres, M. E., Barry, J. P., Hubbard, D. A., & Suess, E. (2001). Reconstructing the history of fluid flow at cold seep sites from Ba/Ca ratios in vesicomyid clam shells. *Limnology and Oceanography*, *46*(7), 1701–1708.

Torres, M. E., Mix, A. C., & Rugh, W. D. (2005). Precise δ13C analysis of dissolved inorganic carbon in natural waters using automated headspace sampling and continuous-flow mass spectrometry. Limnol. Oceanogr. *Methods*, *3*(8), 349–360.

Usapkar, A., Dewangan, P., Kocherla, M., Ramprasad, T., Mazumdar, A., & Ramana, M. V. (2014). Enhanced methane flux event and sediment dispersal pattern in the Krishna–Godavari offshore basin: Evidences from rock magnetic techniques. *Marine and Petroleum Geology*, *58*, 461–475.

Usui, Y. (2015). *Data report: Rock magnetism of sediment from IODP Expedition 334 Sites U1378 and U1379. In Vannucchi, P., Ujiie, K., Stroncik, N., Malinverno, A., and the Expedition 334 Scientists, Proc. IODP, 334*. Tokyo: Integrated Ocean Drilling Program Management International, Inc. https://doi.org/10.2204/iodp.proc.334.203.2015

Vannucchi, P., Galeotti, S., Clift, P. D., Ranero, C., & von Huene, R. (2004). Long term subduction erosion along the Middle America Trench offshore Guatemala. *Geology*, *32*(7), 617–620.

Vannucchi, P., Morgan, J. P., Silver, E. A., & Kluesner, J. W. (2016). Origin and dynamics of depositionary subduction margins. Geochemi. *Geophys., Geosyst.*, *17*(6), 1966–1974.

Vannucchi, P., Sak, P. B., Morgan, J. P., Ohkushi, K., Ujiie, K., & Scientists, I. E. S. (2013). Rapid pulses of uplift, subsidence, and subduction erosion offshore Central America: Implications for building the rock record of convergent margins. *Geology*, *41*, 995–998.

Vannucchi, P., Ujiie, K., Stroncik, N., & Malinverno, A. (2012). and the Expedition 334 Scientists. In *Proc. IODP, 334*. Tokyo: Integrated Ocean Drilling Program Management International, Inc. https://doi.org/10.2204/iodp.proc.334.103.2012

Zhang, M., Konishi, H., Xu, H., Sun, X., Lu, H., Wu, D., & Wu, N. (2014). Morphology and formation mechanism of pyrite induced by the anaerobic oxidation of methane from the continental slope of the NE South China Sea. *Journal of Asian Earth Sciences*, *92*, 293–301.